

# Calibration-Free Accelerated Dynamic MRI based on Low-Rank Matrix Recovery

M. Salman Asif  
Rice University

Justin Romberg  
Georgia Institute of Technology

Richard Baraniuk  
Rice University

**Abstract**—Parallel magnetic resonance (MR) imaging techniques use multiple receiver coils for data acquisition. Sensitivity responses of these coils usually vary in space and must be estimated via a separate calibration process. We present an algorithm for jointly estimating MR images and coil sensitivity maps from subsampled k-space measurements. We pose the joint estimation problem as the recovery of a rank-one matrix from coded, linear measurements. We demonstrate the performance of our method on cardiac MRI datasets with multiple receiver coils.

## I. MOTIVATION

Accelerated MRI techniques reduce acquisition time by sampling only a fraction of k-space. Parallel MR imaging techniques utilize information provided by multiple receiver coils with varying spatial profiles and recover images from undersampled k-space data provided by each receiver [1]. However, the coil sensitivity responses need to be measured for proper image reconstruction. Typically, a separate scan is performed for calibration purposes, which increases the total acquisition time. The goal of calibration-free methods is to recover MR images directly from the under-sampled k-space data without performing a separate scan for calibration.

## II. PROBLEM FORMULATION

Consider a parallel, dynamic MRI system that contains  $C$  receiver coils and observes a sequence with  $T$  images. The measurements acquired by a coil  $c$  at time  $t$  can be written as

$$\mathbf{y}_t^c = \mathbf{R}_{\Omega_t} \mathbf{F}(\mathbf{s}_c \odot \mathbf{x}_t), \quad (1)$$

where  $\mathbf{x}_t$  denotes an  $N \times D$  complex-valued MR image,  $\mathbf{s}_c$  denotes an  $N \times D$  coil sensitivity map,  $\odot$  denote element-wise multiplication,  $\mathbf{F}$  denotes 2D discrete Fourier transform operator, and  $\mathbf{R}_{\Omega_t}$  denotes a downsampling operator on the Fourier (k-space) data along a trajectory denoted by  $\Omega_t$  that yield the measurement vector  $\mathbf{y}_t^c$ . In our experiments, we use phase-encoding along cartesian trajectory; in particular, we sample  $M$  rows out of the  $N \times D$  k-space and denote  $R = N/M$  as the acceleration factor. However, the method can be generalized to arbitrary sampling trajectories.

We can describe a linear system of measurements for all the coils and MR frames in a rank-one matrix form as follows. Let us first denote the measurements corresponding to the MR image  $\mathbf{x}_t$  as

$$\begin{bmatrix} \mathbf{y}_t^1 \\ \mathbf{y}_t^2 \\ \vdots \\ \mathbf{y}_t^c \end{bmatrix} = \begin{bmatrix} \mathbf{R}_{\Omega_t} \mathbf{F} & \mathbf{0} & \dots & \mathbf{0} \\ \mathbf{0} & \mathbf{R}_{\Omega_1} \mathbf{F} & \dots & \mathbf{0} \\ \vdots & \vdots & \ddots & \vdots \\ \mathbf{0} & \mathbf{0} & \dots & \mathbf{R}_{\Omega_t} \mathbf{F} \end{bmatrix} \begin{bmatrix} \mathbf{s}_1 \odot \mathbf{x}_t \\ \mathbf{s}_2 \odot \mathbf{x}_t \\ \vdots \\ \mathbf{s}_c \odot \mathbf{x}_t \end{bmatrix} \quad (2)$$

$$\equiv \mathbf{y}_t = \mathcal{A}_t(\mathbf{x}_t \mathbf{s}^*), \quad (3)$$

where  $\mathbf{s}$  denotes a vector of size  $CND$  that contains all the coil sensitivity maps,  $\{\mathbf{s}_c\}_{c=1}^C$ ;  $\mathcal{A}_t$  denotes an operator that performs Fourier transform and subsampling on the diagonal entries of the submatrices  $[\mathbf{x}_t \mathbf{s}_1^* \quad \mathbf{x}_t \mathbf{s}_2^* \quad \dots \quad \mathbf{x}_t \mathbf{s}_C^*]$  in the rank-one matrix  $\mathbf{x}_t \mathbf{s}^*$ .

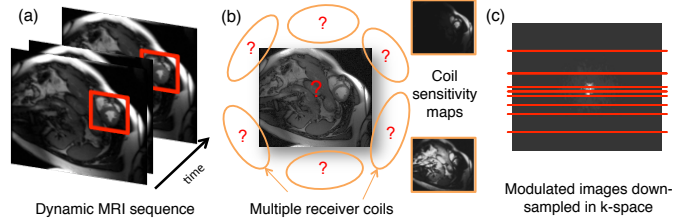


**Fig. 1:** Motivation. (a) A sequence of images in a dynamic MRI sequence (red bounding boxes denote the region that contains most of the temporal variations). (b) Receiver coils have spatially varying sensitivity responses. (c) Modulated images are subsampled in k-space (Fourier domain) for acceleration. Our goal is to reconstruct the MR images from subsampled k-space data without the knowledge of coil sensitivity maps.

Similarly, by combining all the  $\mathbf{y}_t$ , we can write the complete system of measurements as

$$\mathbf{y} = \mathcal{A}(\mathbf{x} \mathbf{s}^*), \quad (4)$$

where  $\mathbf{x}$  denotes a vector of size  $TND$  that concatenates all the MR images,  $\{\mathbf{x}_t\}_{t=1}^T$ ;  $\mathcal{A}$  denotes an operator that performs Fourier transform and subsampling on all the diagonal blocks of the rank-one matrix  $\mathbf{x} \mathbf{s}^*$  and yields the measurement vector  $\mathbf{y}$  of size  $TCMD$ .

The system in (4) corresponds to linear measurements of a rank-one matrix in which  $\mathbf{x}$ ,  $\mathbf{s}$  appear in a bilinear form. We jointly estimate  $\mathbf{x}$  and  $\mathbf{s}$  by posing the estimation problem as the low-rank matrix recovery from coded, linear measurements [2]. Instead of using the nuclear norm as a proxy for low rank and solving a semidefinite program, we solve the following optimization problem, based on low-rank factorization and augmented Lagrangian method in [3]:

$$\min_{\mathbf{X}, \mathbf{S}} \|\mathbf{X}\|_F^2 + \|\mathbf{S}\|_F^2 \quad \text{s.t.} \quad \mathbf{y} = \mathcal{A}(\mathbf{X} \mathbf{S}^*), \quad (5)$$

where  $\mathbf{X}$  and  $\mathbf{S}$  represent low-rank matrices of size  $TND \times L$  and  $CND \times L$ , respectively, and  $L$  is a small number close to the rank of the unknown matrix, which in our case is one. This problem can also be viewed as multi-channel blind deconvolution in which a signal of interest  $\hat{\mathbf{x}}$  passes through different, unknown channels  $\hat{\mathbf{s}}$  before being sampled using multiple receivers [4].

In addition to the rank-one structure in (4), we can exploit multiple spatial and temporal redundancies in dynamic MRI. For instance, in dynamic MR images (e.g., cardiac MRI), changes occur only in a small part of the image (e.g., beating heart), while the rest of the image remains static. To exploit this temporal structure, we can divide each image in the sequence  $\{\mathbf{x}_t\}_{t=1}^T$  into static and dynamic regions (i.e.,  $\mathbf{x}_t = [\mathbf{x}_t^{\text{static}} \mid \mathbf{x}_t^{\text{dynamic}}]$ ), such that the static regions are fixed in all  $\mathbf{x}_t$  and the dynamic regions change from frame to frame. We can easily incorporate such a partition in (4) and (5) by including an operator that maps static and dynamic parts to the complete image sequence. An advantage of such partitioning is that the number of

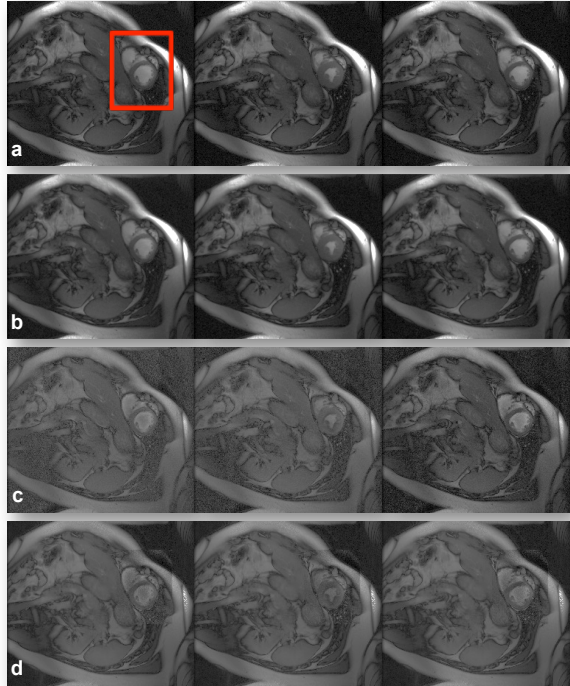


**Fig. 2:** Reconstruction results for short-axis scan with  $R = 4$ . **(a)** Fully sampled MR images. **(b,c,d)** Images reconstructed from subsampled k-space. **(b)** Uses known sensitivity maps in (5). **(c)** Jointly estimates MR images and coil sensitivities in (5). **(d)** Uses static and dynamic partitions in (5). Images reconstructed while jointly estimating coil sensitivity maps, shown in (c,d), have comparable quality to those reconstructed with perfect knowledge of coil sensitivity maps, as shown in (b).

unknowns reduce by the same factor as the number of pixels in the static region.

### III. EXPERIMENTS

In our experiments, we simulated an accelerated imaging setup by downsampling full k-space data from multiple receiver coils; detailed description of these datasets can be found in [5]. We present reconstructed images for a short-axis MRI scan with  $R = 4$  in Fig. 2 and a two-chamber view cine MRI scan with  $R = 8$  in Fig. 3. The size of the short-axis dataset is  $N = 224, D = 256, T = 16$ , and the two-chamber dataset is  $N = 240, D = 200, T = 20$ ; both datasets were acquired with  $C = 5$  element cardiac coil. In both datasets, we subsampled k-space for each frame by first selecting 8 center rows and then randomly selecting a total of  $M$  rows to achieve the acceleration factor  $R = N/M$ .

The results are presented in Fig. 2 and Fig. 3. Fig. 2(a) and Fig. 3(a) present three images selected from the respective sequences that were reconstructed from fully sampled k-space data and known estimates of the respective sensitivity maps. Fig. 2(b) and Fig. 3(b) present images reconstructed from the down-sampled k-space data and known estimates of the sensitivity maps in a least-squares problem. Fig. 2(c) and Fig. 3(c) present images reconstructed by solving (5) jointly for the MR images and the coil sensitivity maps. Fig. 2(d) and Fig. 3(d) present images reconstructed by solving (5) with static and dynamic partition in  $\mathbf{X}$ . For the short-axis scan in Fig. 2 we designated  $100 \times 75$  pixels (the region inside the red bounding box in Fig. 2(a)) as the dynamic part, which implies that the rest of the image remains

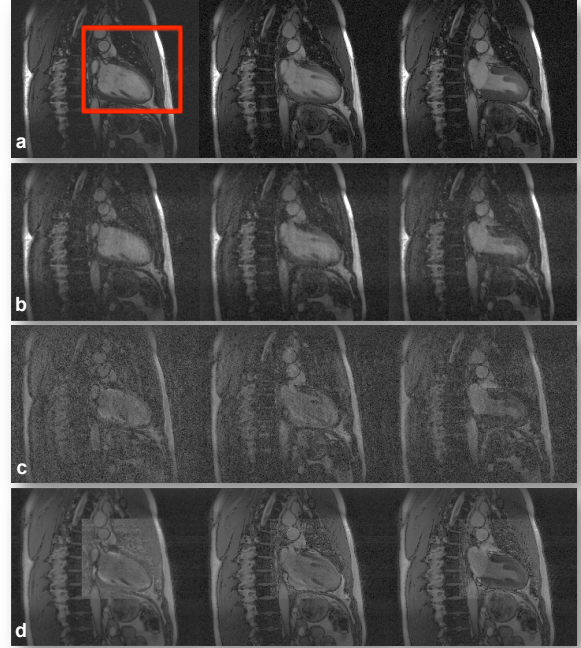


**Fig. 3:** Reconstruction results for two-chamber scan with  $R = 8$ . **(a)** Fully sampled MR images. **(b,c,d)** Images reconstructed from subsampled k-space. **(b)** Uses known sensitivity maps in (5). **(c)** Jointly estimates MR images and coil sensitivities in (5); these images are noisy because of large  $R$ . **(d)** Uses static and dynamic partitions in (5); these images have comparable quality to those reconstructed with perfect knowledge of coil sensitivity maps, as shown in (b). The brightness difference between static and dynamic regions in (d) can be easily fixed in a post-processing step.

unchanged in all the frames. For the two-chamber scan in Fig. 3, we used  $100 \times 100$  pixels (highlighted in Fig. 3(a)) as the dynamic part.

The images reconstructed with exact sensitivity maps, as shown Fig. 2(b) and Fig. 3(b), can be considered the best reference that we can achieve while jointly estimating the images and coil sensitivity maps. We observed that the low-rank matrix reconstruction based method for jointly estimating coil sensitivities and MR images provides comparable reconstruction for  $R = 4$  (compare Fig. 2 (b) and (c)). Adding static-dynamic partitions in (5) makes the reconstruction for  $R = 8$  comparable as well (compare Fig. 3 (b) and (d)).

We expect that including additional spatial regularization and motion-adaptive constraints (similar to those in [5]) can further improve the quality of reconstruction, and we intend to pursue that in future work.

### IV. COMPARISON WITH EXISTING AUTOCALIBRATION METHODS

A number of existing autocalibration schemes use cross-relation consistency for estimating coil response filters in a multichannel system. Consider the following multichannel model. Suppose we observe a signal  $x$  using an array of filters  $h_{i=1,2,\dots,N}$  as

$$y_i = x \otimes h_i.$$

The cross-relation consistency suggests that

$$y_i \otimes h_j = y_j \otimes h_i \quad \text{for all } i, j = 1, \dots, N. \quad (6)$$

The null-space of the matrix defined by these equations provides all the feasible solutions. We expand the system in (6) as follows.

$$\begin{bmatrix} \mathcal{C}_{y_1} & -\mathcal{C}_{y_2} & 0 & \dots & 0 \\ \mathcal{C}_{y_1} & 0 & -\mathcal{C}_{y_3} & \dots & 0 \\ \mathcal{C}_{y_1} & 0 & 0 & \dots & -\mathcal{C}_{y_N} \\ -\mathcal{C}_{y_1} & \mathcal{C}_{y_2} & 0 & \dots & 0 \\ 0 & \mathcal{C}_{y_2} & -\mathcal{C}_{y_3} & \dots & 0 \\ 0 & \mathcal{C}_{y_2} & 0 & \dots & -\mathcal{C}_{y_N} \\ \vdots & \vdots & \vdots & \ddots & \vdots \\ -\mathcal{C}_{y_1} & 0 & 0 & \dots & \mathcal{C}_{y_N} \\ 0 & -\mathcal{C}_{y_2} & 0 & \dots & \mathcal{C}_{y_N} \\ 0 & 0 & -\mathcal{C}_{y_3} & \dots & \mathcal{C}_{y_N} \end{bmatrix} \begin{bmatrix} h_1 \\ h_2 \\ h_3 \\ \vdots \\ h_N \end{bmatrix} = 0, \quad (7)$$

where  $\mathcal{C}_{y_k}$  denotes a circulant/toeplitz matrix created with  $y_k$ . However, this scheme only works in the case of fully-sampled data.

Most of the existing MRI auto-calibration schemes use sidmilar ideas to perform the coil calibration. A typical example of auto-calibration in MRI involves learning a set of filters  $g_{c,k}$  such that

$$y_c = \sum_k g_{c,k} \otimes y_k, \quad (8)$$

where  $y_c$  denotes the k-space corresponding to the  $c$ th coil,  $g_{c,1}, \dots, g_{c,C}$  denotes a set of filters that reproduce any sample in  $y_c(r)$  using all the samples within a small neighborhood  $\mathcal{N}(\nabla)$ , in all the coils, such that  $g_{c,c}(r) = 0$ .

Consider the following simple conversion from the cross-relation model in (6) to the SPIRIT auto-calibration model in (8): Note that we can us first describe the conversion matrix by

#### REFERENCES

- [1] K. P. Pruessmann, M. Weiger, M. B. Scheidegger, and P. Boesiger, "SENSE: Sensitivity encoding for fast MRI," *Magnetic resonance in medicine*, vol. 42, no. 5, pp. 952–962, 1999.
- [2] B. Recht, M. Fazel, and P. A. Parrilo, "Guaranteed minimum-rank solutions of linear matrix equations via nuclear norm minimization," *SIAM Review*, vol. 52, no. 3, pp. 471–501, 2010.
- [3] S. Burer and R. D. Monteiro, "A nonlinear programming algorithm for solving semidefinite programs via low-rank factorization," *Mathematical Programming*, vol. 95, no. 2, pp. 329–357, 2003.
- [4] A. Ahmed, B. Recht, and J. Romberg, "Blind deconvolution using convex programming," *IEEE Trans. Info. Theory*, vol. 60, no. 3, pp. 1711–1732, March 2014.
- [5] M. S. Asif, L. Hamilton, M. Brummer, and J. Romberg, "Motion-adaptive spatio-temporal regularization for accelerated dynamic MRI," *Magnetic Resonance in Medicine*, vol. 70, no. 3, pp. 800–812, 2013.